Nuclear Charge Radii of Silicon Isotopes

Kristian König,[1,2,*] Julian C. Berengut,[3] Anastasia Borschevsky,[4] Alex Brinson,[5] B. Alex Brown,[1,6] Adam Dockery,[1,6] Serdar Elhatisari,[7,8] Ephraim Eliav,[9] Ronald F. Garcia Ruiz,[5,†] Jason D. Holt,[10,11] Bai-Shan Hu,[12,13] Jonas Karthein,[5] Dean Lee,[1,6] Yuan-Zhuo Ma,[1,6] Ulf-G. Meißner,[8] Kei Minamisono,[1,6,‡] Alexander V. Oleynichenko,[14,15] Skyy V. Pineda,[1,16,§] Sergey D. Prosnyak,[14,17] Marten L. Reitsma,[4] Leonid V. Skripnikov,[14,17] Adam Vernon,[5] and Andréi Zaitsevskii[14,18]

[1]*Facility for Rare Isotope Beams, Michigan State University, East Lansing, Michigan 48824, USA*
[2]*Technische Universität Darmstadt, 64289 Darmstadt, Germany*
[3]*School of Physics, University of New South Wales, NSW 2052, Australia*
[4]*University of Groningen, 9747 Groningen, Netherlands*
[5]*Massachusetts Institute of Technology, Department of Physics, Cambridge, Massachusetts 02139, USA*
[6]*Department of Astronomy and Physics, Michigan State University, East Lansing, Michigan 48824, USA*
[7]*Faculty of Natural Sciences and Engineering, Gaziantep Islam Science and Technology University, Gaziantep 27010, Turkey*
[8]*Helmholtz-Institut für Strahlen- und Kernphysik and Bethe Center for Theoretical Physics, Universität Bonn, D-53115 Bonn, Germany*
[9]*School of Chemistry, Tel Aviv University, 69978 Tel Aviv, Israel*
[10]*TRIUMF, Vancouver, British Columbia V6T 2A3, Canada*
[11]*Department of Physics, McGill University, Montreal, Quebec H3A 2T8, Canada*
[12]*National Center for Computational Sciences, Oak Ridge National Laboratory, Oak Ridge, Tennessee 37831, USA*
[13]*Physics Division, Oak Ridge National Laboratory, Oak Ridge, Tennessee 37831, USA*
[14]*Petersburg Nuclear Physics Institute named by B. P. Konstantinov of NRC "Kurchatov Institute," Gatchina 188300, Russia*
[15]*Moscow Institute of Physics and Technology, Institutsky lane 9, Dolgoprudny, Moscow region, 141700, Russia*
[16]*Department of Chemistry, Michigan State University, East Lansing, Michigan 48824, USA*
[17]*Saint Petersburg State University, 7/9 Universitetskaya nab., St. Petersburg 199034, Russia*
[18]*Department of Chemistry, M. V. Lomonosov Moscow State University, Leninskie gory 1/3, Moscow 119991, Russia*

(Received 6 September 2023; revised 12 January 2024; accepted 26 February 2024; published 16 April 2024; corrected 9 July 2024)

The nuclear charge radius of ^{32}Si was determined using collinear laser spectroscopy. The experimental result was confronted with *ab initio* nuclear lattice effective field theory, valence-space in-medium similarity renormalization group, and mean field calculations, highlighting important achievements and challenges of modern many-body methods. The charge radius of ^{32}Si completes the radii of the mirror pair ^{32}Ar-^{32}Si, whose difference was correlated to the slope L of the symmetry energy in the nuclear equation of state. Our result suggests $L \leq 60$ MeV, which agrees with complementary observables.

DOI: 10.1103/PhysRevLett.132.162502

Introduction.—Recent advances in many-body methods, the continuous increase in computing power, and the development of internucleon potentials derived from chiral effective field theory, are leading up to a new era of precision nuclear theory calculations with quantifiable uncertainties [1–3]. Besides the description of diverse nuclear properties, even extremely neutron-rich matter, such as neutron stars, can now be addressed [4,5].

The properties of neutron stars are governed by the nuclear equation of state (EOS) and affect, for instance, the forms of gravitational waves from a binary neutron star merger [6] or the character of super heavy nuclei [7]. However, despite the broad experimental efforts, the form of the EOS, especially the slope L in the symmetry energy, could only be constrained to a limited range [8–10] insufficient for precise model predictions. An alternative approach to constrain L based on the concept of charge symmetry of the nuclear interaction was suggested recently. It uses the differences of charge radii of a pair of mirror nuclei as a proxy for the neutron-skin thickness [11–13], for which the correlation on L was discussed in [14–18]. Enhanced sensitivity is expected thanks to possibly large isospin asymmetry if one of the mirror nuclei is a radioactive nucleus [12,19], hence contrasting most previous studies on stable nuclei due to technical reasons.

Despite the compelling progress in nuclear theory, significant long-standing challenges persist in our understanding of nuclei [20]. For instance, obtaining a simultaneous description of the binding energy and nuclear charge radii has proven to be a major challenge [20–23]. Moreover, it is still unclear if effective theories constrained to a finite number of nuclei can provide reliable calculations of infinite nuclear matter at supersaturation density [5,12,24,25]. Therefore, precision measurements of charge radii for nuclei with large proton-to-neutron asymmetries are critical in guiding the progress of nuclear theory and the description of nuclear matter.

The investigation of nuclear charge radii of Si isotopes ($Z = 14$), in particular, highlights several questions of great interest. The charge radius of ^{32}Si, measured in this work, sets a new constraint on L when combined with data of its mirror partner ^{32}Ar [26]. Furthermore, nuclear charge radii of Si isotopes play a critical role in studies of the appearance or disappearance of nuclear magic numbers [27,28] and the emergence of exotic nuclear shapes, e.g., bubble nuclei [29,30]. From the theoretical side, recent progress was made in calculating these properties by several many-body methods [20,30].

However, previous to our work, only measurements for the nuclear charge radii of stable silicon isotopes were available [31,32]. This is partly because nuclear charge radius measurements of short-lived Si isotopes pose major challenges in production and extraction from the thick targets of isotope separator online facilities. Moreover, silicon is a highly reactive element and likely to form molecular compounds unsuitable for laser spectroscopy experiments. Here, we present charge radius measurements of ^{32}Si obtained from collinear laser spectroscopy of ^{28,29,30,32}Si isotopes after the molecular breakup of SiO molecules. The experiment was performed at the BECOLA setup at the Facility for Rare Isotope Beams.

Experiment.—The stable ^{28,29,30}Si isotopes used as a reference for the isotope shift measurements were produced as bare singly charged ions in a Penning-ionization gauge ion source [33] with cathodes of natural silicon. The radioactive ^{32}Si ($T_{1/2} = 153$ y, $I = 0^+$) beam was generated with an oven-ion source, which is based on target-ion source modules developed at CERN/ISOLDE, for the batch mode ion source (BMIS) system [34]. The radioactive ^{32}Si was purchased and chemically processed [34,35] to convert it to a compound, which has lower melting point, and finally loaded to the oven-ion source. The beam, generated ~20 m upstream of BECOLA, first went through a dipole magnet for mass selection. Because of a 1000∶1 contamination of ^{32}S relative to ^{32}Si at mass 32, a mass-48 beam was selected instead. At 1300 °C, this mass component was the most populated from the BMIS and contained mostly singly charged ^{32}Si^{16}O.

At BECOLA [36,37], the ions were first fed into a helium-gas-filled radio-frequency quadrupole (RFQ) ion trap [38] floated at a potential of 29 813 V. The helium-buffer gas pressure was set to 120 mTorr. Since the beam energy from the ion sources was 30 keV, the injection energy into the RFQ was about 190 eV. This injection energy was sufficient to break the SiO molecules by collisions with the helium-buffer gas to be left with bare singly charged Si ions required for laser spectroscopy. At a 100 V lower injection energy, no laser spectroscopy signal was observed due to a low dissociation efficiency. At a 100 V higher injection energy, the stopping efficiency in the RFQ was decreased, and only a weak resonance signal was observed. The resulting bare singly charged Si ions were cooled by collisions with the helium-buffer gas and then extracted as a continuous beam.

Since Si^+ ions are not accessible by laser spectroscopy due to the lack of transitions in the optical regime, the ions were first neutralized with Na vapor inside the charge-exchange cell (CEC) [39]. The CEC was heated to 410 °C, leading to a 50% neutralization efficiency of the incoming ion beam. During the charge exchange process, many electronic states are populated and redistributed through spontaneous decays. In this cascade decay, low-lying metastable states tend to be populated. One of these metastable states ($3s^2 3p^2\,^1S_0$, 15 394.370 cm^{-1} [40]) was used as the lower state for the laser spectroscopy. Based on a simulation [33], about 2% of the total population reached this $^1S_0$ state at the time atoms arrived in the fluorescence detection region (FDR) installed 70 cm downstream of the CEC.

The atoms in the $3s^2 3p^2\,^1S_0$ state were excited with laser light at 391 nm to the $3s^2 3p 4s\,^1P_1^o$ state at 40 991.884 cm^{-1}. With a probability of 93%, the excited electrons decay at 288 nm to the $3s^2 3p^2\,^1D_2$ state at 6298.850 cm^{-1} [40], which allowed us to perform laser-background-free spectroscopy by eliminating the scattered 391-nm light. Therefore, we used a Hamamatsu H11870-09 photomultiplier tube (PMT) with a quantum efficiency of ≈7% at 288 nm but a 4 orders of magnitude lower sensitivity at 391 nm. Additionally, we placed an absorption filter (Hoya U340) in front of the PMT, which transmits more than 50% of the UV light but absorbs 99.8% of the scattered 391-nm laser light. The fluorescence light was collected with an elliptical mirror with MIRO coating from ALANOD, which is highly reflective for the deep UV light. The PMT was placed outside the vacuum chamber at the second focal point. To achieve resonance between atom and laser frequency, Doppler tuning was applied. The atom velocity was altered by applying a small scanning potential difference of < 50 V to the CEC, causing Doppler shifts of the transition frequency, while the laser frequency was kept constant. The employed laser was a continuous-wave Ti-sapphire laser (Matisse TS, Sirah Lasertechnik) operated at 782 nm and pumped by a frequency-doubled Nd-YAG solid-state laser (Millennia eV, Spectra Physics). The 782-nm light was guided to a cavity-based frequency doubler (Wavetrain, Spectra Physics), creating the 391-nm light. This light was transported via an optical fiber to the beamline and irradiated in collinear geometry. In front of the optical fiber, an acousto-optical modulator was used to block the laser beam. Spectroscopy was performed with a laser power of 4 mW and a laser-beam diameter of 2 mm at the interaction region. The short-term frequency stabilization was realized via side-of-fringe locking to a reference cavity. For long-term stabilization, the cavity length was controlled by feedback from a wavelength meter (WSU30, High-Finesse) calibrated every minute to a helium-neon laser (SL 03, SIOS Meßtechnik).

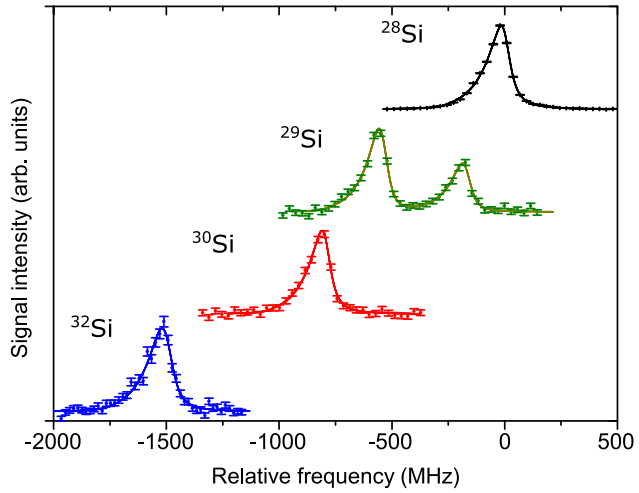

FIG. 1. Normalized resonance spectra of ^{28,29,30,32}Si. Inelastic collisions during the charge exchange process led to slightly asymmetric line shapes and were considered in the fit function [39]. The frequency is relative to the centroid of ^{28}Si.

To avoid optical depopulation along the 70 cm flight path between CEC and FDR by the strong UV decay, the acousto-optical modulator was used to chop the laser beam so that only unprobed atoms were excited in the FDR. A continuous ion beam was chosen over a bunched beam to avoid uncertainties caused by a varying temporal overlap between the ion bunch with a time spread of typically 1 μs and the time width of the laser (0.3 μs). More details on the experimental method are presented in the Supplemental Material [41]. Examples of the measured spectra are shown in Fig. 1. For the isotope ^{29}Si with nuclear spin $I = 1/2$, the measured hyperfine splitting allowed the determination of the magnetic hyperfine parameter $A_{\text{upper}} = -252.5(6)$ MHz. To reduce systematic contributions (e.g., from the wavelength meter), at least five different laser-frequency sets at different beam energies were measured as detailed in [64]. The results are listed in Table I with statistical (first parentheses) and systematical uncertainties (second parentheses, same as in [64]) together with the literature values of the nuclear charge radii of the stable isotopes [31].

The present isotope shifts and absolute radii [31] were used in a King fit procedure [65] to extract the mass and field-shift constants, $K^{(\text{MS})}$ and $F^{(\text{el})}$. The limited amount of reference isotopes, however, restricted the accuracy, particularly for $F^{(\text{el})}$. Hence, additional atomic calculations (method A, details can be found in the Supplemental Material) were utilized to constrain the field-shift parameter in the King fit to $F^{(\text{el})} = 97.0(8)$ MHz/fm^2. From the combined King fit, a mass-shift parameter of $K^{(\text{MS})} = -340.8(1.4)$ GHz u was extracted, which enabled a reliable determination of nuclear charge radii. Additional independent atomic calculations confirmed the determined atomic parameters (see Table II in the Supplemental Material). Applying the atomic factors from the combined King fit reduced the uncertainty of $R(^{32}\text{Si})$ by a factor of 2.6 compared to the unconstrained King fit.

TABLE I. Measured isotope shifts $\delta\nu^{A,28} = \nu^A - \nu^{28}$ relative to ^{28}Si with statistical and systematical uncertainties, differential $\delta\langle r^2\rangle$, and absolute R_{ch} charge radii. The R_{ch} and $\delta\langle r^2\rangle^{A,28}$ of the stable $^{28-30}$Si isotopes and the $R_{\text{ch}}(^{32}\text{Ar})$ are taken from [31]. The charge radius of ^{32}Si was extracted from the isotope shift and the atomic factors deduced from the constrained King fit, see text.

	$\delta\nu^{A,28}$ (MHz)	$\delta\langle r^2\rangle^{A,28}$ (fm^2)	R_{ch} (fm)
^{28}Si	0	0	3.1224 (24)
^{29}Si	−425.1 (1.1) (2.1)	−0.030 (36)	3.1176 (52)
^{30}Si	−805.0 (1.1) (2.1)	0.070 (29)	3.1336 (40)
^{32}Si	−1505.3 (3.1) (2.1)	0.195 (76)	3.153 (12)
^{32}Ar	⋯	⋯	3.3468 (62)

Nuclear charge radii vs nuclear theory.—The extracted atomic factors were used to determine the differential mean square charge radius $\delta\langle r^2\rangle$, using the expression

$$\delta\langle r^2\rangle^{A,A'} = \frac{\delta\nu^{A,A'} - \mu^{A,A'}K^{(\text{MS})}}{F^{(\text{el})}}, \tag{1}$$

with $\mu^{A,A'} = (m_A - m_{A'})/[(m_A + m_e)(m_{A'} + m_e)]$, where $m_{A,A'}$ and m_e are the atomic masses of Si and the electron mass, respectively. With the isotope shift given in Table I, we obtained $\delta\langle r^2\rangle^{32,28} = 0.195(76)$ fm^2, resulting in a charge radius of $R(^{32}\text{Si}) = 3.153(12)$ fm. Figure 2 compares the experimental findings with theoretical results from three different complementary many-body methods: (i) density

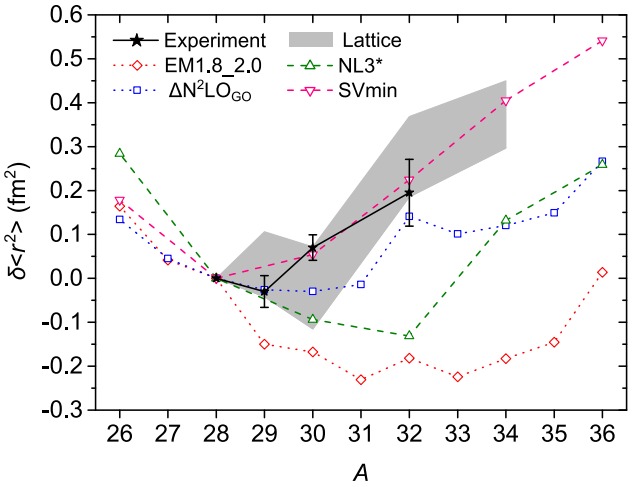

FIG. 2. Experimental and theoretical differential mean square charge radii of Si. Only the nuclear lattice calculation provided an uncertainty, which is plotted as a gray band. Together with the DFT calculations using the SVmin functional, the lattice results agree with the experimental results.

function calculations (DFT) using two functionals, NL3* and SVmin, [66,67]; (ii) valence-space in-medium similarity renormalization group (VS-IMSRG) calculations [68–70] using two parametrizations of the internucleon interaction, EM1.8_2.0, which generally reproduces ground-state energies well, but underpredicts absolute charge radii [71,72], and $\Delta\,\mathrm{N^2LO_{GO}}(394)$, including explicit Δ degrees of freedom showing an improved description of radii [73]; and (iii) nuclear lattice effective field theory calculations [20]. Further details of the calculations are included in the Supplemental Material.

As seen in Fig. 2, the theoretical results exhibit diverging trends as a function of the neutron number. Within uncertainties, the lattice and the DFT calculation using the SVmin functional show a good agreement with the experiment. Interestingly, VS-IMSRG results with the EM1.8_2.0 interaction deviate from the experimental trend in contrast to other regions of the nuclear chart where the same interaction has provided a good description of differential charge radii [23,74,75]. The calculations with the $\Delta\,\mathrm{N^2LO_{GO}}(394)$ interaction are closer to the experimental data, especially with ^{28,29,32}Si, but fall short in reproducing ^{30}Si. Furthermore, the VS-IMSRG results predict very different trends beyond $A = 32$ compared to lattice and DFT. A major recent achievement of nuclear lattice calculations has been the description of absolute nuclear charge radii [20]. Such absolute results are shown in Fig. 5 in the Supplemental Material. Other recent results using nuclear lattice calculations can be found in Refs. [76–78]. The VS-IMSRG calculations significantly underestimate the nuclear size, which is an unsolved challenge for most of the *ab initio* calculations of medium and heavy mass nuclei, largely stemming from the input chiral interactions themselves [22,23,79]. On the other hand, DFT calculations using the SVmin functional overestimate the radii, while the NL3* functional yields good overall radii but misses the experimental trend.

Mirror radii and nuclear matter.—Within the DFT framework, the sensitivity of the mirror charge radii difference, $\Delta R_{\mathrm{ch}} = R_{\mathrm{p}}(N,Z) - R_{\mathrm{p}}(Z,N)$, to L, was found to be correlated with $|N-Z| \times L$ [8,12,13], where N and Z are the neutron and proton numbers, respectively. This correlation has already been applied to set constraints on L in ^{36}Ca-^{36}S, ^{38}Ca-^{38}Ar [80] and ^{54}Ni-^{54}Fe [81] pairs. Since the nuclear charge radius of ^{32}Ar is known [26], our measurement of ^{32}Si completes the ^{32}Ar-^{32}Si pair with $|N-Z| = 4$. The experimental values are listed in Table I, and yield $\Delta R_{\mathrm{ch}} = R_{\mathrm{ch}}(^{32}\mathrm{Si}) - R_{\mathrm{ch}}(^{32}\mathrm{Ar}) = 0.194(14)$ fm.

To illustrate the correlation between ΔR_{ch} and L, DFT calculations were performed for 48 Skyrme energy-density functionals [82], and the results are shown in Fig. 3. The colors in the figure indicate the assumed values for the neutron skin of ^{208}Pb: 0.12 fm (red), 0.16 fm (orange), 0.20 fm (green), and 0.24 fm (blue). These calculations are analogous to those carried out for the $A = 36$ mirror pair

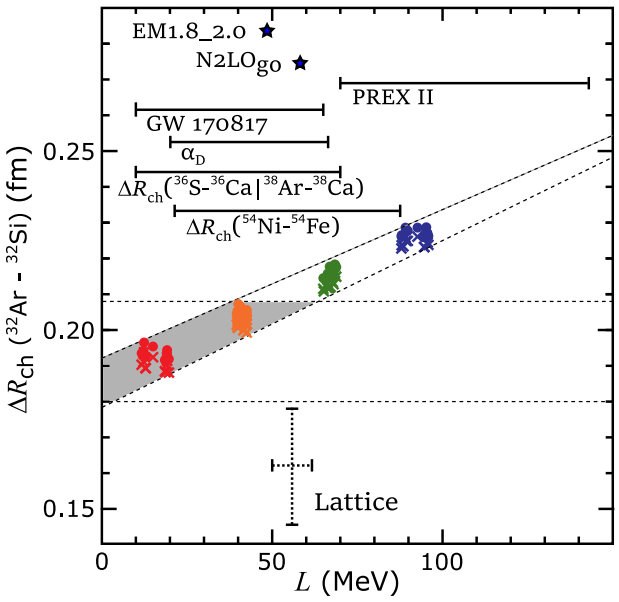

FIG. 3. $\Delta R_{\mathrm{ch}}(^{32}\mathrm{Ar} - {}^{32}\mathrm{Si})$ as a function of L. The experimental 1σ constraint of ΔR_{ch} is indicated by the horizontal dashed lines. The solid circles are the results of Skyrme energy-density functionals, and the crosses are for the covariant density functional calculations. The overlapping area, highlighted in gray, shows our constraint for $L \leq 60$ MeV. It is in good agreement with the result from the ^{54}Ni-^{54}Fe [81], the ^{36}Ca-^{36}S, and the ^{38}Ca-^{38}Ar mirror pairs [80], with the findings from the electric dipole polarizability α_{D} [85], the neutron star merger GW170817 [84] but smaller than the PREX II result [83]. Please note that those are only plotted as reference on the L axis and are not correlated to ΔR_{ch}. From our theoretical calculations on the lattice and from VS-IMSRG calculations with the EM1.8_2.0 and $\Delta\,\mathrm{N^2LO_{GO}}$ interaction, we deduced ΔR_{ch} and related those with corresponding calculations for L [20,25,73].

^{36}Ca-^{36}S in [80], and are described in the Supplemental Material. The correlation and our extracted value of ΔR_{ch} yield a constraint of $L \leq 60$ MeV. As a reference, other experimental constraints of L are shown in the figure without meaning of their y-axis position. These constraints come from the Pb neutron-skin thickness (PREX II) [83], the GW170817 binary neutron star merger [84], the nuclear electric dipole polarizability α_{D} [85], and the ^{36}Ca-^{36}S, ^{38}Ca-^{38}Ar, ^{54}Ni-^{54}Fe mirror-pair radii [80,81]. Our result agrees well with most of the other findings. However, the PREX II evaluation from Ref. [83] indicates a stiffer nuclear EOS. For comparison, our theoretical results for ΔR_{ch} and L from lattice and VS-IMSRG calculations are depicted in Fig. 3. As VS-IMSRG calculations are not developed yet to calculate properties of nuclear matter, we used our calculated charge radii differences and literature values of L using the $\Delta\,\mathrm{N^2LO_{GO}}$ and EM1.8_2.0 interactions [25,73]. The VS-IMSRG calculations overestimate ΔR_{ch}, while the lattice calculations yield a slightly smaller value, mainly due to an underestimation of $R_{\mathrm{ch}}(^{32}\mathrm{Ar})$

compared to experimental data. The results for L, however, are in good agreement with complementary calculations available in the literature, such as quantum Monte Carlo [86,87], energy density functionals [88,89], chiral effective field theory calculations [5], and a combined analysis of astrophysical data with PREX II and chiral effective field theory [90]. All of those theoretical results agree with our experimental constraint of $L \leq 60$ MeV.

Conclusions and outlook.—We performed collinear laser spectroscopy of ^{28,29,30,32}Si by extracting SiO molecules from the BMIS source that were broken in the BECOLA RFQ. The nuclear charge radius of ^{32}Si was determined and provides an essential benchmark for the development of theoretical models. Our experimental result is in good agreement with *ab initio* lattice predictions and DFT calculations using the SVmin functional. In contrast to the results for different regions of the nuclear chart [23,79], VS-IMSRG calculations fall short of reproducing the charge radii of silicon isotopes. Beyond $A = 32$, the applied theoretical models significantly deviate in their trends, motivating further research of neutron-rich silicon isotopes. The silicon isotopic chain further exhibits unique features that make these nuclear systems particularly challenging and attractive for our understanding of the nuclear many-body problem. Of special future interest is the study of the suggested "doubly magic" nuclei ^{34}Si [91] and ^{42}Si [28,92], as well as the suggested "bubble" structure in ^{34}Si [29,30,93].

The present radius of ^{32}Si, combined with the literature value of ^{32}Ar, allowed testing the correlation between the nuclear mirror radii differences and the slope of the symmetry energy of the equation of state of the nuclear matter. The result suggests a value of $L \leq 60$ MeV, which is in good agreement with constraints obtained from other mirror pairs [80,81] and different experimental observables, such as gravitational waves of the binary neutron star merger [6] and nuclear reactions [94,95]. Hence, mirror charge radius measurements provide a complementary electromagnetic probe to those from accelerator-based terrestrial experiments and astronomical observations. Our results, also inferred from gravitational wave observations, suggest a softer EOS. As theoretical understanding deepens, and experimental precision improves, we will be able to combine multiple independent results of difference of mirror charge radii to obtain a tighter constraint on L. We believe that the development of the lattice calculations in this study represents a significant step forward in resolving the theoretical model dependence.

The constraints on L can be improved with further precision studies of the ^{32}Ar-^{32}Si mirror pair. As the current limitations are the atomic parameters needed to deduce the charge radius from the isotope shift, precise muonic x-ray spectroscopy in ^{29,30}Si would lead to significant improvements. Furthermore, muonic measurements on thin targets were recently demonstrated [96]. We hope our results could motivate the extension of these measurements to ^{32}Si. Moreover, a future charge radius measurement of the neutron-deficient isotope ^{22}Si could be combined with its mirror ^{22}O to form their mirror radii difference with the largest proton-neutron asymmetry $|N - Z| = 6$ of all reasonably accessible pairs at the Facility for Rare Isotope Beams, thus resulting in a higher sensitivity to L. Assuming the same precision for $\Delta R_{\mathrm{ch}}(^{22}\mathrm{Si} - ^{22}\mathrm{O})$ as obtained for $\Delta R_{\mathrm{ch}}(^{32}\mathrm{Ar} - ^{32}\mathrm{Si})$ would translate into an improvement of precision of L by a factor of 2.

This work was supported in part by the National Science Foundation under Grants No. PHY-21-11185 and No. PHY-21-10365, and the U.S. Department of Energy under the Grants No. DE-SC0021176, No. DE-SC0021152, No. DE-SC0013365, No. DE-SC0023658, SciDAC-5 NUCLEI Collaboration. Calculations of isotope shift constants have been supported by the Russian Science Foundation Grant No. 19-72-10019-P. We thank the Center for Information Technology of the University of Groningen for their support and for providing access to the Peregrine high-performance computing cluster. J. K. acknowledges the support of a Feodor Lynen Fellowship of the Alexander-von-Humboldt Foundation. Y. Z. M. was supported by the National Natural Science Foundation of China under Grant No. 12105106 and China Postdoctoral Science Foundation under Grant No. BX20200136. The work of U. G. M. and S. E. was supported in part by the European Research Council (ERC) under the European Union's Horizon 2020 research and innovation program (Grant Agreement No. 101018170). The work of U. G. M. was further supported by VolkswagenStiftung (Grant No. 93562) and by the CAS President's International Fellowship Initiative (PIFI) (Grant No. 2018DM0034). For the lattice calculations, we acknowledge computational resources provided by the Oak Ridge Leadership Computing Facility through the INCITE award "*Ab initio* nuclear structure and nuclear reactions," the Southern Nuclear Science Computing Center, the Gauss Centre for Supercomputing e.V. for computing time on the GCS Supercomputer JUWELS at the Jülich Supercomputing Centre (JSC), and the Institute for Cyber-Enabled Research at Michigan State University. VS-IMSRG calculations are supported by NSERC under Grants No. SAPIN-2018-00027 and No. RGPAS-2018-522453 as well as the Arthur B. McDonald Canadian Astroparticle Physics Research Institute. We thank S. R. Stroberg for the IMSRG++ code [97] used to perform these calculations. Computations were performed with an allocation of computing resources on Cedar at WestGrid and the Digital Research Alliance of Canada.

*kkoenig@ikp.tu-darmstadt.de
†rgarciar@mit.edu
‡minamiso@frib.msu.edu
§Present address: KU Leuven, 3000 Leuven, Belgium.

[1] E. Epelbaum, H.-W. Hammer, and U.-G. Meißner, Rev. Mod. Phys. **81**, 1773 (2009).
[2] H. Hergert, Front. Phys. **8**, 379 (2020).
[3] B. Hu, W. Jiang, T. Miyagi, Z. Sun, A. Ekström, C. Forssén, G. Hagen, J. D. Holt, T. Papenbrock, S. R. Stroberg, and I. Vernon, Nat. Phys. **18**, 1196 (2022).
[4] C. D. Capano, I. Tews, S. M. Brown, B. Margalit, S. De, S. Kumar, D. A. Brown, B. Krishnan, and S. Reddy, Nat. Astron. **4**, 625 (2020).
[5] C. Drischler, R. J. Furnstahl, J. A. Melendez, and D. R. Phillips, Phys. Rev. Lett. **125**, 202702 (2020).
[6] B. P. Abbot *et al.* (LIGO Scientific and Virgo Collaborations), Phys. Rev. Lett. **119**, 161101 (2017).
[7] W. Nazarewicz, Nat. Phys. **14**, 537 (2018).
[8] X. Roca-Maza and N. Paar, Prog. Part. Nucl. Phys. **101**, 96 (2018).
[9] C. J. Horowitz, E. F. Brown, Y. Kim, W. G. Lynch, R. Michaels, A. Ono, J. Piekarewicz, M. B. Tsang, and H. H. Wolter, J. Phys. G **41**, 093001 (2014).
[10] X. Vinas, M. Centelles, X. Roca-Maza, and M. Warda, Eur. Phys. J. A **50**, 27 (2014).
[11] N. Wang and T. Li, Phys. Rev. C **88**, 011301(R) (2013).
[12] B. A. Brown, Phys. Rev. Lett. **119**, 122502 (2017).
[13] J. Yang and J. Piekarewicz, Phys. Rev. C **97**, 014314 (2018).
[14] P.-G. Reinhard and W. Nazarewicz, Phys. Rev. C **105**, L021301 (2022).
[15] B. A. Brown and K. Minamisono, Phys. Rev. C **106**, L011304 (2022).
[16] Y. N. Huang, Z. Z. Li, and Y. F. Niu, Phys. Rev. C **107**, 034319 (2023).
[17] R. An, S. Sun, L.-G. Cao, and F.-S. Zhang, Nucl. Sci. Tech. **34**, 119 (2023).
[18] P. Bano, S. P. Pattnaik, M. Centelles, X. Viñas, and T. R. Routray, Phys. Rev. C **108**, 015802 (2023).
[19] J. Piekarewicz, Phys. Rev. C **83**, 034319 (2011).
[20] S. Elhatisari, L. Bovermann, E. Epelbaum, D. Frame, F. Hildenbrand, M. Kim, Y. Kim, H. Krebs, T. A. Lähde, D. Lee, N. Li, B.-N. Lu, Y. Ma, U.-G. Meißner, G. Rupak, S. Shen, Y.-H. Song, and G. Stellin, arXiv:2210.17488.
[21] A. Ekström, G. R. Jansen, K. A. Wendt, G. Hagen, T. Papenbrock, B. D. Carlsson, C. Forssén, M. Hjorth-Jensen, P. Navrátil, and W. Nazarewicz, Phys. Rev. C **91**, 051301(R) (2015).
[22] R. F. Garcia Ruiz *et al.*, Nat. Phys. **12**, 594 (2016).
[23] R. de Groote, J. Billowes, C. Binnersley, M. Bissell, T. Cocolios, T. Day Goodacre, G. Farooq-Smith, D. Fedorov, K. Flanagan, S. Franchoo, R. Garcia Ruiz, W. Gins, J. Holt, A. Koszorus, T. Miyagi, W. Nazarewicz, G. Neyens, P. Reinhard, and X. Yang, Nat. Phys. **16**, 620 (2020).
[24] M. B. Tsang, J. R. Stone, F. Camera, P. Danielewicz, S. Gandolfi, K. Hebeler, C. J. Horowitz, J. Lee, W. G. Lynch, Z. Kohley, R. Lemmon, P. Möller, T. Murakami, S. Riordan, X. Roca-Maza, F. Sammarruca, A. W. Steiner, I. Vidaña, and S. J. Yennello, Phys. Rev. C **86**, 015803 (2012).
[25] G. Hagen, A. Ekström, C. Forssén, G. R. Jansen, W. Nazarewicz, T. Papenbrock, K. A. Wendt, S. Bacca, N. Barnea, B. Carlsson, C. Drischler, K. Hebeler, M. Hjorth-Jensen, M. Miorelli, G. Orlandini, A. Schwenk, and J. Simonis, Nat. Phys. **12**, 186 (2016).
[26] A. Klein, B. A. Brown, U. Georg, M. Keim, P. Lievens, R. E. Neugart, M. Neuroth, R. Silverans, and L. Vermeeren (ISOLDE Collaboration), Nucl. Phys. **A607**, 1 (1996).
[27] J. Piekarewicz, J. Phys. G **34**, 467 (2007).
[28] J. Fridmann *et al.*, Nature (London) **435**, 922 (2005).
[29] A. Mutschler *et al.*, Nat. Phys. **13**, 152 (2017).
[30] T. Duguet, V. Somà, S. Lecluse, C. Barbieri, and P. Navrátil, Phys. Rev. C **95**, 034319 (2017).
[31] I. Angeli and K. Marinova, At. Data Nucl. Data Tables **99**, 69 (2013).
[32] X. Yang, S. Wang, S. Wilkins, and R. Garcia Ruiz, Prog. Part. Nucl. Phys. **129**, 104005 (2023).
[33] C. Ryder, K. Minamisono, H. Asberry, B. Isherwood, P. Mantica, A. Miller, D. Rossi, and R. Strum, Spectrochim. Acta Part B At. Spectrosc. **113**, 16 (2015).
[34] C. Sumithrarachchi *et al.*, Nucl. Instrum. Methods Phys. Res., Sect. B **541**, 301 (2023).
[35] K. A. Domnanich, S. Satija, V. S. Bodnar, G. Bollen, C. R. Kleinfeldt, Y. Liu, S. Rogers, S. Schwarz, G. W. Severin, C. Sumithrarachchi, and A. C. Villari, Appl. Radiat. Isot. **200**, 110958 (2023).
[36] K. Minamisono, P. Mantica, A. Klose, S. Vinnikova, A. Schneider, B. Johnson, and B. Barquest, Nucl. Instrum. Methods Phys. Res., Sect. A **709**, 85 (2013).
[37] D. M. Rossi, K. Minamisono, B. R. Barquest, G. Bollen, K. Cooper, M. Davis, K. Hammerton, M. Hughes, P. F. Mantica, D. J. Morrissey, R. Ringle, J. A. Rodriguez, C. A. Ryder, S. Schwarz, R. Strum, C. Sumithrarachchi, D. Tarazona, and S. Zhao, Rev. Sci. Instrum. **85**, 093503 (2014).
[38] B. Barquest, G. Bollen, P. Mantica, K. Minamisono, R. Ringle, S. Schwarz, and C. Sumithrarachchi, Nucl. Instrum. Methods Phys. Res., Sect. A **866**, 18 (2017).
[39] A. Klose, K. Minamisono, C. Geppert, N. Frömmgen, M. Hammen, J. Krämer, A. Krieger, C. Levy, P. Mantica, W. Nörtershäuser, and S. Vinnikova, Nucl. Instrum. Methods Phys. Res., Sect. A **678**, 114 (2012).
[40] NIST, NIST Atomic Spectra Database Lines Form (2023).
[41] See Supplemental Material at http://link.aps.org/supplemental/10.1103/PhysRevLett.132.162502 for more experimental details and a description of the employed atomic and nuclear theory calculations, which includes Refs. [42–63].
[42] K. R. Anton, S. L. Kaufman, W. Klempt, G. Moruzzi, R. Neugart, E. W. Otten, and B. Schinzler, Phys. Rev. Lett. **40**, 642 (1978).
[43] A. S. P. Gomes *et al.*, DIRAC, a relativistic *ab initio* electronic structure program, see http://diracprogram.org (accessed on 4 February 2022), Release DIRAC19 (2019).
[44] R. Saue *et al.*, J. Chem. Phys. **152**, 204104 (2020).
[45] K. G. Dyall, Theor. Chem. Acc. **135**, 128 (2016).
[46] A. Landau, E. Eliav, and U. Kaldor, *Intermediate Hamiltonian Fock-Space Coupled-Cluster Method* (Academic Press, New York, 2001), Vol. 39, pp. 171–188.
[47] F. P. Gustafsson *et al.*, Phys. Rev. A **102**, 052812 (2020).
[48] A. V. Oleynichenko, A. Zaitsevskii, and E. Eliav, in *Supercomputing*, edited by V. Voevodin and S. Sobolev (Springer

International Publishing, Cham, 2020), Vol. 1331, pp. 375–386.
[49] A. V. Oleynichenko, A. Zaitsevskii, L. V. Skripnikov, and E. Eliav, Symmetry **12**, 1101 (2020).
[50] V. M. Shabaev, Theor. Math. Phys. **63**, 588 (1985).
[51] C. W. P. Palmer, J. Phys. B **20**, 5987 (1987).
[52] V. M. Shabaev, Sov. J. Nucl. Phys. **47**, 69 (1988).
[53] V. M. Shabaev and A. N. Artemyev, J. Phys. B **27**, 1307 (1994).
[54] G. Penyazkov, S. D. Prosnyak, A. E. Barzakh, and L. V. Skripnikov, J. Chem. Phys. **158**, 114110 (2023).
[55] E. V. Kahl and J. C. Berengut, Comput. Phys. Commun. **238**, 232 (2019).
[56] V. A. Dzuba, V. V. Flambaum, and M. G. Kozlov, Phys. Rev. A **54**, 3948 (1996).
[57] J. Z. Han, C. Pan, K. Y. Zhang, X. F. Yang, S. Q. Zhang, J. C. Berengut, S. Goriely, H. Wang, Y. M. Yu, J. Meng, J. W. Zhang, and L. J. Wang, Phys. Rev. Res. **4**, 033049 (2022).
[58] Y.-Z. Ma, Z. Lin, B.-N. Lu, S. Elhatisari, D. Lee, N. Li, U.-G. Meißner, A. W. Steiner, and Q. Wang, arXiv:2306.04500.
[59] T. Miyagi, S. R. Stroberg, P. Navrátil, K. Hebeler, and J. D. Holt, Phys. Rev. C **105**, 014302 (2022).
[60] K. Hebeler, S. K. Bogner, R. J. Furnstahl, A. Nogga, and A. Schwenk, Phys. Rev. C **83**, 031301(R) (2011).
[61] N. Shimizu, T. Mizusaki, Y. Utsuno, and Y. Tsunoda, Comput. Phys. Commun. **244**, 372 (2019).
[62] B. A. Brown and W. A. Richter, Phys. Rev. C **74**, 034315 (2006).
[63] B. A. Brown, Phys. Rev. C **58**, 220 (1998).
[64] K. König, F. Sommer, J. Lantis, K. Minamisono, W. Nörtershäuser, S. Pineda, and R. Powel, Phys. Rev. C **103**, 054305 (2021).
[65] W. H. King, *Isotope Shifts in Atomic Spectra* (Springer Science+Business Media, New York, 1984).
[66] S. E. Agbemava, A. V. Afanasjev, D. Ray, and P. Ring, Phys. Rev. C **89**, 054320 (2014).
[67] P. Klüpfel, P.-G. Reinhard, T. J. Bürvenich, and J. A. Maruhn, Phys. Rev. C **79**, 034310 (2009).
[68] S. R. Stroberg, A. Calci, H. Hergert, J. D. Holt, S. K. Bogner, R. Roth, and A. Schwenk, Phys. Rev. Lett. **118**, 032502 (2017).
[69] S. R. Stroberg, S. K. Bogner, H. Hergert, and J. D. Holt, Annu. Rev. Nucl. Part. Sci. **69**, 307 (2019).
[70] T. Miyagi, S. R. Stroberg, J. D. Holt, and N. Shimizu, Phys. Rev. C **102**, 034320 (2020).
[71] J. Simonis, S. R. Stroberg, K. Hebeler, J. D. Holt, and A. Schwenk, Phys. Rev. C **96**, 014303 (2017).
[72] S. R. Stroberg, J. D. Holt, A. Schwenk, and J. Simonis, Phys. Rev. Lett. **126**, 022501 (2021).
[73] W. G. Jiang, A. Ekström, C. Forssén, G. Hagen, G. R. Jansen, and T. Papenbrock, Phys. Rev. C **102**, 054301 (2020).
[74] S. Malbrunot-Ettenauer *et al.*, Phys. Rev. Lett. **128**, 022502 (2022).
[75] F. Sommer *et al.*, Phys. Rev. Lett. **129**, 132501 (2022).
[76] B.-N. Lu, N. Li, S. Elhatisari, D. Lee, J. E. Drut, T. A. Lähde, E. Epelbaum, and U.-G. Meißner, Phys. Rev. Lett. **125**, 192502 (2020).
[77] B.-N. Lu, N. Li, S. Elhatisari, Y.-Z. Ma, D. Lee, and U.-G. Meißner, Phys. Rev. Lett. **128**, 242501 (2022).
[78] S. Shen, S. Elhatisari, T. A. Lähde, D. Lee, B.-N. Lu, and U.-G. Meißner, Nat. Commun. **14**, 2777 (2023).
[79] Á. Koszorús *et al.*, Nat. Phys. **17**, 439 (2021).
[80] B. A. Brown *et al.*, Phys. Rev. Res. **2**, 022035(R) (2020).
[81] S. V. Pineda, K. König, D. M. Rossi, B. A. Brown, A. Incorvati, J. Lantis, K. Minamisono, W. Nörtershäuser, J. Piekarewicz, R. Powel, and F. Sommer, Phys. Rev. Lett. **127**, 182503 (2021).
[82] B. A. Brown, Phys. Rev. Lett. **111**, 232502 (2013).
[83] B. T. Reed, F. J. Fattoyev, C. J. Horowitz, and J. Piekarewicz, Phys. Rev. Lett. **126**, 172503 (2021).
[84] C. A. Raithel and F. Özel, Astrophys. J. **885**, 121 (2019).
[85] X. Roca-Maza, X. Viñas, M. Centelles, B. K. Agrawal, G. Colò, N. Paar, J. Piekarewicz, and D. Vretenar, Phys. Rev. C **92**, 064304 (2015).
[86] A. W. Steiner and S. Gandolfi, Phys. Rev. Lett. **108**, 081102 (2012).
[87] S. Gandolfi, J. Carlson, S. Reddy, A. Steiner, and R. Wiringa, Eur. Phys. J. A **50**, 10 (2013).
[88] P.-G. Reinhard, X. Roca-Maza, and W. Nazarewicz, Phys. Rev. Lett. **127**, 232501 (2021).
[89] P.-G. Reinhard, X. Roca-Maza, and W. Nazarewicz, Phys. Rev. Lett. **129**, 232501 (2022).
[90] R. Essick, I. Tews, P. Landry, and A. Schwenk, Phys. Rev. Lett. **127**, 192701 (2021).
[91] P. Baumann, A. Huck, G. Klotz, A. Knipper, G. Walter, G. Marguier, H. Ravn, C. Richard-Serre, A. Poves, and J. Retamosa, Phys. Lett. B **228**, 458 (1989).
[92] B. Bastin *et al.*, Phys. Rev. Lett. **99**, 022503 (2007).
[93] J. Yao, H. Mei, and Z. Li, Phys. Lett. B **723**, 459 (2013).
[94] M. B. Tsang, J. R. Stone, F. Camera, P. Danielewicz, S. Gandolfi, K. Hebeler, C. J. Horowitz, J. Lee, W. G. Lynch, Z. Kohley, R. Lemmon, P. Möller, T. Murakami, S. Riordan, X. Roca-Maza, F. Sammarruca, A. W. Steiner, I. Vidaña, and S. J. Yennello, Phys. Rev. C **86**, 015803 (2012).
[95] C. Y. Tsang, M. B. Tsang, W. G. Lynch, R. Kumar, and C. J. Horowitz, Nat. Astron. **8**, 328 (2024).
[96] A. Adamczak *et al.*, Eur. J. Phys. A **59**, 15 (2023).
[97] S. R. Stroberg, https://github.com/ragnarstroberg/imsrg.

Correction: A miscommunication during the proof cycle led to incorrect reference numbering, which has now been rectified. The Supplemental Material has also been replaced to coordinate with the correct reference numbering.